Energy Harvesting From Hybrid Indoor Ambient Light and Thermal Energy Sources for Enhanced Performance of Wireless Sensor Nodes

Yen Kheng Tan, *Student Member, IEEE*, and Sanjib Kumar Panda, *Senior Member, IEEE*

***Abstract*—In this paper, a hybrid of indoor ambient light and thermal energy harvesting scheme that uses only one power management circuit to condition the combined output power harvested from both energy sources is proposed to extend the lifetime of the wireless sensor node. By avoiding the use of individual power management circuits for multiple energy sources, the number of components used in the hybrid energy harvesting (HEH) system is reduced and the system form factor, cost and power losses are thus reduced. An efficient microcontroller-based ultra low power management circuit with fixed voltage reference based maximum power point tracking is implemented with closed-loop voltage feedback control to ensure near maximum power transfer from the two energy sources to its connected electronic load over a wide range of operating conditions. From the experimental test results obtained, an average electrical power of 621 μW is harvested by the optimized HEH system at an average indoor solar irradiance of 1010 lux and a thermal gradient of 10 K, which is almost triple of that can be obtained with conventional single-source thermal energy harvesting method.**

***Index Terms*—Hybrid energy harvesting (HEH), near maximum power point tracking (MPPT), solar and thermal energy sources, wireless sensor nodes.**

I. Introduction

In MANY wireless systems such as Wireless Sensor Network (WSN), the life span and performance of the wireless sensor node and communication circuits are very important. However, these factors are largely limited by the size and/or weight constraints of their on-board energy storage devices like batteries [1], which have limited energy capacity to sustain the WSN nodes for an extended period of time. Roundy *et al.* [2] illustrate that given a 1 cm^3 of primary battery (0.8 Wh/cm^3) volume, the sensor node, with an average power consumption of 100 μW, can only last for around 11 months before the node goes into idle state. As such, the concept of energy harvesting from readily available energy sources present in the ambient environment [3]–[7] such as solar energy, thermal energy, wind energy, and vibration energy directly at the deployed site to supplement and recharge the energy storage devices for powering the sensor nodes has been introduced. Many energy harvesting systems have already been developed and those reported in the literature are mostly for outdoor applications where solar energy is plentiful. Very few research works [8], [9] have discussed the indoor energy harvesting from ambient light source, which has serious challenges to resolve.

Indoor energy harvesting for sustaining low-power electronic remote sensors for supervisory and alarm system is illustrated in this paper. There are two main challenges associated with indoor energy harvesting: 1) ambient energy sources in the indoor environment are very weak, hence the harvested power is much lower than that of the outdoor condition; and 2) availability of energy sources are dependent on the indoor environmental conditions. According to Randall *et al.* [10], it has been shown that the light intensity of artificial lighting conditions found in hospitals and office buildings is only a small fraction of the light intensity for outdoor sun of 100–1000 W/m^2. As such, the power density of an amorphous solar cell with efficiency of $< 10\%$ under indoor light intensity of < 10 W/m^2 is significantly reduced to 100 $\mu W/cm^2$ [11]. This is even more challenging when indoor energy harvesting is available for a limited period of time. The ambient energy sources can be intermittent and inconsistent at times depending on the indoor environmental conditions. Take for example, indoor lighting is only available during office hours and almost complete darkness for the rest of the day. Because these challenges related to the weak and uncertain energy sources, energy harvesting in indoor environment from a single energy source might not be adequate to sustain the operation or even to enhance the performance of the miniaturized wireless sensor nodes over the lifetime.

In this paper, the concept of energy harvesting from two readily available indoor energy sources, i.e., ambient light energy from artificial lighting and thermal energy from machines heat, is proposed to overcome the drawbacks of single source energy harvesting in order to extend the lifespan of a wireless sensor node. Tadesse *et al.* [12] and Khaligh *et al.* [13], for example, have presented a mechanical structure made up of two different energy harvesting mechanisms on the same platform to harvest from the same vibration energy source. Other hybrid energy harvesting (HEH) approaches discussed in [14]–[16] focus on different power management schemes to harvest multiple energy sources. Guilar *et al.* [14] and Lhermet *et al.* [15] propose to combine energy harvesting using an electronic switch/multiplexer to switch between two energy sources. Whenever both energy sources are present simultaneously, based on the priority given by the power management circuit, only one of

Manuscript received June 27, 2010; revised October 2, 2010; accepted November 9, 2010. Date of publication December 23, 2010; date of current version August 12, 2011.

The authors are with the Department of Electrical and Computer Engineering, National University of Singapore, Singapore 117576 (e-mail: tanyenkheng@ieee.org; eleskp@nus.edu.sg).

Color versions of one or more of the figures in this paper are available online at http://ieeexplore.ieee.org.

Digital Object Identifier 10.1109/TIE.2010.2102321

TABLE I
CHARACTERISTICS OF INDOOR ENERGY SOURCES

Energy source	Characteristics	Comments
Solar	Intermittent	Illumination from artificial lighting during office hours
Wind	Continuous	Air circulation from air conditioner and electric fans
Thermal	Continuous/ Intermittent	Thermal gradient between body, machine heat and ambient
Vibration	Intermittent	Vibration from machine and human motion during walking, running, etc.

TABLE II
PERFORMANCE OF ENERGY HARVESTERS UNDER INDOOR CONDITIONS (ADAPTED FROM [17])

Energy Harvester	Power Densities	
	Indoor condition	*Outdoor condition*
Solar panel	$100\mu W/cm^2$ @10W/cm^2	10mW/cm^2 @STC
Wind turbine-generator	35μW/cm^2 @<1m/s	3.5mW/cm^2 @8.4m/s
Thermoelectric generator	100μW/cm^2 @5^{o}C gradient	3.5mW/cm^2 @30^{o}C gradient
Electromagnetic generator	4μW/cm^3 @human motion-Hz 800μW/cm^3 @machine-kHz	

the two energy sources would then be harvested. Hence, it is not possible to harvest energy from both energy sources simultaneously. To overcome the drawback, Park *et al.* [16] introduces an HEH system, AmbiMax, that harvests simultaneously from multiple energy sources to sustain the operation of the sensor nodes. Each energy source is allocated to charge its own supercapacitor and the energy stored in these supercapacitors is then transferred to the lithium-ion battery.

Although simultaneous charging from multiple energy sources can be achieved, the drawback with AmbiMax [16] is that each energy harvesting source requires its own unique power management unit i.e., DC-DC converter and associated circuitry to condition the power flow from the source to the output load. As more energy sources are combined together, the number of power management unit for each individual energy source increases, hence more components are needed and larger volumetric size, higher power losses, and higher costs are incurred. Emphasis of this paper is placed on enhancing the performance of the wireless sensor node deployed in the challenging indoor context using HEH from solar and thermal energy sources. A near maximum power point tracking (MPPT) technique is explored for the HEH system to maximize power transfer from the hybrid energy sources to the sensor node.

The rest of the paper is organized as follows: Section II illustrates the energy harvesting methodology for indoor wireless sensor node. Section III discusses how the solar and thermal EH systems are combined using separate power electronic-based converters. Following that, the optimized HEH system using a single power management unit for indoor wireless sensor node prototype is illustrated in Section IV, which then ends with a conclusion and discussions in Section V.

II. ENERGY HARVESTING METHODOLOGY FOR INDOOR WIRELESS SENSOR NODE

A. Overview of Indoor Energy Sources

The characteristics and performances of the renewable energy sources available in outdoor environmental conditions are very different from those found in indoor industrial, commercial and biomedical environments. Within the enclosed environment like offices, hospitals, factories, etc., the energy sources are generally generated by some artificial means. Table I shows a summary of the indoor energy sources and their characteristics.

Referring to Table I, it can be seen that the artificial energy sources found in indoor environment are generated from electrical appliances such as artificial lightings, air conditioners, machines, etc. and human movement. Each of these appliances and human bodies has its own primary purpose. For example, artificial lighting and air conditioner are primarily used to generate light for visual function and air circulation for cooling purposes. During the normal operation of these electrical appliances and human movements, some stray energies are generated for energy harvesting. The availability of the artificial energy sources seen in Table I is largely dependent on the operational schedules of the electrical appliances and the lifestyles of the human beings. For some energy sources such as solar and vibration, they are only available at times according to the intermittent operating profile of the artificial lighting, machine operation, and human movement. Conversely, the wind and thermal energy sources exist in continuous form as the air conditioners and machineries of indoor industrial, commercial or biomedical environment are operated at a duty cycle close to 100%.

Apart from the issue of availability of energy sources, another concern is the power harvesting throughput. The power densities of various energy harvesting technologies per unit cm^2 or cm^3 are recorded in Table II. Under the indoor condition, it can be observed that all the artificial energy sources become very weak. The power density of a solar panel, for example, with efficiency of $< 10\%$ under the indoor solar irradiance of 10 W/m^2 is only 100 μW/cm^2 as compared to 10 mW/cm^2 under the outdoor standard testing condition. Table II shows that the average power that can be harvested by all the artificial energy sources is 10–100 times lower than that of the outdoor ambient energy sources. As such, these weak and uncertain indoor energy sources pose significant challenges on energy harvesting from a single energy source for sustaining the operation of the wireless sensor nodes over the entire lifetime.

To enhance the performance of the wireless sensor node in indoor environment, HEH from solar and thermal energy sources is proposed in this paper. Among the various artificial energy sources, solar and thermal energy sources share similar high power densities as can be seen in Table II. In addition, the undesirable intermittent solar energy sources found in offices or factories lightings can be supplemented by the continuous thermal energy supply from waste heat generated by

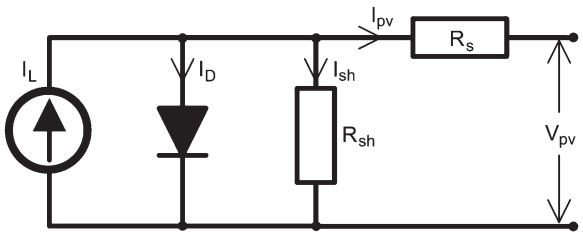

Fig. 1. Equivalent electrical circuit for a photovoltaic module.

machineries. Whenever solar energy is not available, instead of solely relying on the energy stored in the on-board energy storage devices proposed by Nasiri *et al.* and Hande *et al.* in [8] and [9], respectively, an alternate approach is to harvest from the readily available thermal energy source to continue powering the operation of the wireless sensor node before exhausting the energy stored in the energy storage device. Another key characteristic of the proposed HEH system is that the HEH system is able to harvest simultaneously from both energy sources whenever they are available instead of harvesting from individual energy source at one time [12]–[15], hence the performance of the indoor wireless sensor node can be enhanced.

B. Indoor Solar Energy Harvesting System

There exist several mathematical models in the literature [18]–[20] to describe the operation of photovoltaic (PV) cells, from simple to more complex models that account for different reverse saturation currents. In this paper, an electrical circuit with a single diode (single exponential) is considered as the equivalent photovoltaic model, which consists of 15 number of PV cells in series, n_s, as shown in Fig. 1.

Assuming that the shunt resistance, R_{sh}, as shown in Fig. 1, is infinite, the current-voltage (I–V) characteristic of the PV module can be described with a single diode as the four-parameter model given by (1) [18]

$$I_{\rm PV} = I_L - I_o \left[\exp\left(\frac{V_{\rm PV} + I_{\rm PV} R_s}{n_s V_t} \right) - 1 \right] \tag{1}$$

where I_L is the light-generated current (A) and I_o is the dark/reverse saturation current of the p-n diodes (1×10^{-9} A). R_s is the series resistance of the PV module and V_t is the junction terminal thermal voltage (V) depending on the cell absolute temperature, which is defined as

$$V_t = \frac{kT_c}{q} \tag{2}$$

where T_c is the cell absolute temperature (K), k is the Boltzmanns constant (1.3807×10^{-23} JK^{-1}), and q is the charge of the electron (1.6022×10^{-19} C). The ultimate goal is to determine whether the power harvested by the PV module is able to power the wireless sensor node, hence it is crucial to estimate the electrical power throughput of the PV module by leveraging on the relationship between the current and voltage of the PV module expressed by (1). Referring to (1), it can be deduced that the voltage drop across the series resistance, $V_{Rs} = I_{\rm PV} R_s$, is comparably much lower than the output PV voltage, $V_{\rm PV}$, due to the very low PV current, $I_{\rm PV}$, of the order of μA flowing through the small series resistance, R_s, of few Ω, thus the $I_{\rm PV} R_s$ term in (1) can be neglected during the formulation of the output power of the solar panel, $P_{\rm PV}(V_{\rm PV})$, which is expressed as follows:

$$\begin{aligned} P_{\rm PV}(V_{\rm PV}) = V_{\rm PV} I_{\rm PV} &= V_{\rm PV} I_L - V_{\rm PV} I_o \left[\exp\left(\frac{V_{\rm PV}}{n_s V_t} \right) - 1 \right] \\ &\approx V_{\rm PV} I_{\rm sc} - V_{\rm PV} I_o \left[\exp\left(\frac{V_{\rm PV}}{n_s k T_c / q} \right) \right]. \end{aligned} \tag{3}$$

Note that the term $\exp(V_{\rm PV}/n_s V_t) \gg 1$ and the light-generating current, $I_L \approx I_{\rm sc}$, the short circuit current, [18]. The harvested PV power, $P_{\rm PV}(V_{\rm PV})$, as expressed in (3), is formulated as a function of the PV voltage, $V_{\rm PV}$, and it can be simulated based on the technical characteristics of the PV module i.e., n_s, k, q and I_o and the environmental variables such as light irradiance, which is related to I_L, hence $I_{\rm sc}$, and ambient temperature, T_c, of 295 K. For various light irradiance of 380 lux, 425 lux, 480 lux, 640 lux and 1010 lux, the respective $I_{\rm sc}$ are measured to be 60 μA, 65 μA, 74 μA, 96 μA and 150 μA.

For this indoor research work, amorphous type of solar panel, SC-01, especially purchased from Images SI Inc., is for use under indoor conditions i.e., artificial lighting from fluorescent lamps and at room temperature (relatively less variation of temperature at indoor environment than outdoors [10]). At very low light illumination, for example $G = 380$ lux ($\approx 380/120 = 3.17$ W/m^2 [10]), the technical characteristics of the solar panel is tabulated in Table III. The corresponding solar panel's efficiency can also be determined using the following equation given as:

$$\eta = \frac{P_{\rm PV}}{G * A} * 100\%. \tag{4}$$

Based on (4), the efficiency of the solar panel can be calculated to be around 3.4%, which is relatively lower than the outdoor solar panel [11]. Due to the low efficiency of the solar panel in the indoor condition, the power harvested is also low; hence it is necessary to optimize the indoor solar energy harvesting system in order to maximize the power harvested from the solar panel. Further investigations were carried on the solar panel to investigate its performance at different lighting conditions. Figs. 2 and 3 show the indoor solar panel's P–V and P–R curves at different lux illuminations. Both the power curves of the solar panel in relationship with the output voltage (P–V) and the load resistance (P–R) under a range of loads

TABLE III
TECHNICAL CHARACTERISTIC OF SOLAR PANEL USED

Parameter	Unit	Value
Physical dimension	mm	55 x 30 x 1
Cross-sectional area, A	cm^2	16.5
Open circuit voltage, V_{oc} (380 lux)	V	4.14
Short circuit current, I_{sc} (380 lux)	μA	60
MPPT voltage, I_{sc} (380 lux)	V	3.5
MPPT current, I_{sc} (380 lux)	μA	51.44

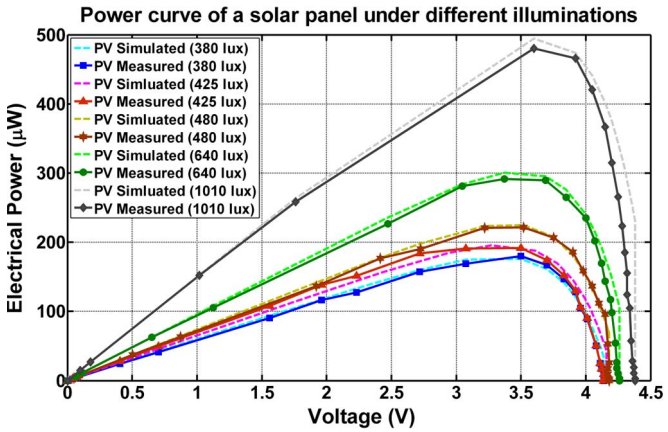

Fig. 2. P–V curves of solar panel at different lux conditions.

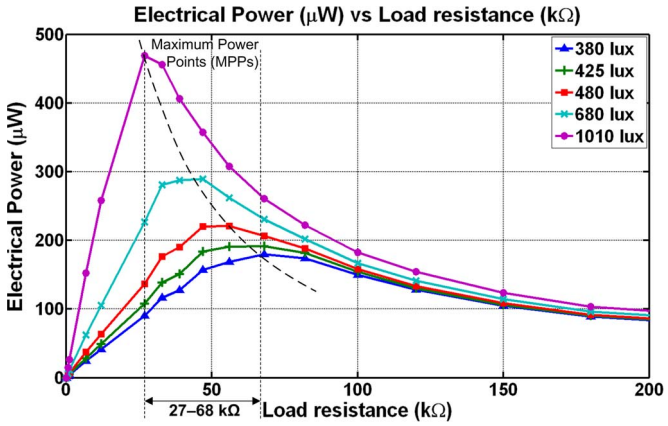

Fig. 3. P–R experimental curves of solar panel at different lux conditions.

from short circuit to open circuit were generated at five different lighting conditions ranging from 380 to 1010 lux.

Taking into consideration the parameters extracted for the solar panel, the model of the solar panel expressed by (3) has been simulated and the simulation results are recorded in Fig. 2. The simulated P–V curves are verified with the measured P–V curves as seen in Fig. 2 for varying solar irradiance conditions, performed by a characterization setup based on a fluorescent light source. Fig. 2 shows that all of the power curves peak near the solar panel output voltage of 3.6 V. In order to compare the characteristics of the solar panel and the thermoelectric generator, the harvested power as a function of the load resistance is plotted as well. For the power curve (P–R) of the solar panel plotted in Fig. 3, it can be observed that the maximum power points (MPPs) of the solar panel vary between 27–68 kΩ. As such, by setting the output voltage of the solar panel fixed at 3.6 V, maximum output power can be harvested from the solar panel under different solar irradiance. Within the indoor lighting conditions of 380–1010 lux, the maximum electrical power that the solar panel can harvest ranges from 180 to 480 μW, respectively.

C. Thermal Energy Harvesting System

In the thermal energy harvesting (TEH) system, a miniaturized thermoelectric generator (TEG) housed in the thermal energy harvester is used for converting thermal energy into

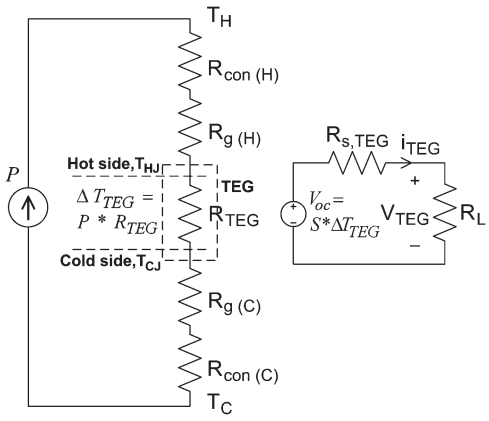

Fig. 4. Equivalent electrical circuit of the thermal energy harvester.

electrical energy. The thermal energy, generated from the heat source at certain high temperature of T_H, is channelled through the enclosed TEG via a thin film of thermally and electrically conductive silver grease between them to the heat sink. The residual heat accumulated in the heat sink is then released to the surrounded ambient air at a lower temperature T_C. An equivalent thermal circuit model of the thermal energy harvester that illustrates its thermal and electrical characteristics is provided in Fig. 4.

Referring to Fig. 4, it can be observed that the temperature difference, $\Delta T_{\rm TEG}$, across the junctions of the TEG is lower than the temperature gradient, $\Delta T = T_H - T_C$, that is externally imposed across the thermal energy harvester. This is because of the thermal contacts and thermal grease resistances residing in the cold and hot sides of the thermal energy harvester i.e., $R_{con(H)}$, $R_{con(C)}$ and $R_{g(H)}$, $R_{g(C)}$, respectively. To minimize this negative effect, the thermal resistance, $R_{\rm TEG}$, of the TEG is made to be as high as possible and/or conversely, the rest of the thermal resistances of the thermal energy harvester are designed to be as small as possible. Taking these design considerations into account, the miniaturized thermal energy harvester, having the physical size of 20 mm × 20 mm × 20 mm, is designed in such a way that most of the heat is channelled through the TEG in order to maximize TEH.

Analysis and characterization works were conducted on the designed thermal energy harvester to evaluate the performance of the TEH system in powering the wireless sensor node. According to Seebeck's effect, the open-circuit voltage, $V_{\rm oc}$, of the TEG enclosed in the thermal energy harvester, which is composed of n thermocouples connected electrically in series and thermally in parallel, is given as

$$V_{\rm oc} = S * \Delta T = n * \alpha (T_H - T_C) \tag{5}$$

where α and S represent the Seebeck's coefficient of a thermocouple and a TEG, respectively. When connecting a load resistance, R_L, electrically to the TEG via the thermal energy harvester as shown in Fig. 4, an electrical current, $I_{\rm TEG}$, flows in accordance to the applied temperature difference, ΔT, which is given as

$$I_{\rm TEG} = \frac{V_{\rm oc} - V_{\rm TEG}}{R_{s,\rm TEG}} = \frac{n * \alpha (T_H - T_C) - V_{\rm TEG}}{R_{s,\rm TEG}} \tag{6}$$

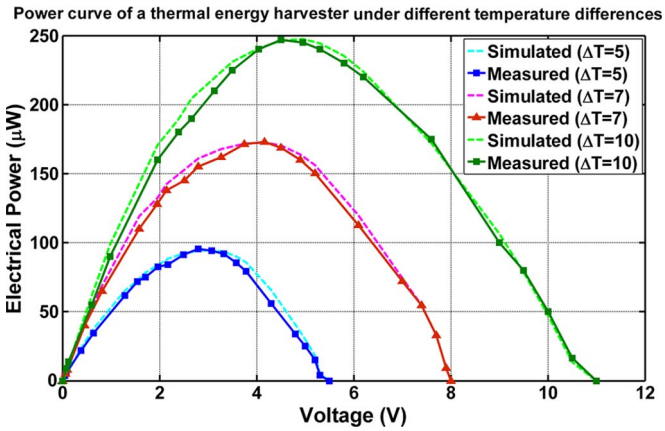

Fig. 5. P–V curves of thermoelectric generator at different thermal gradients.

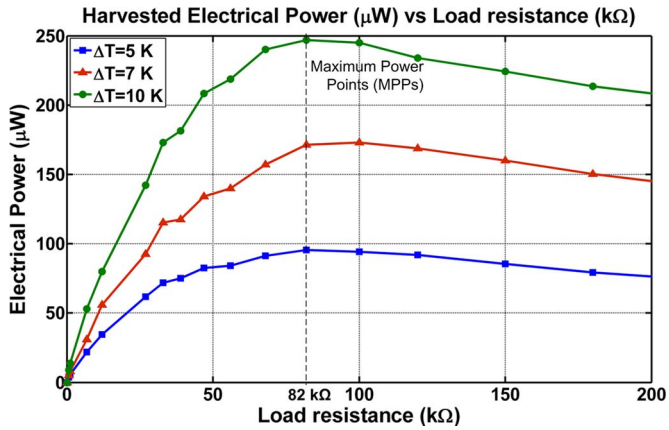

Fig. 6. P–R experimental curves of thermoelectric generator at different thermal gradients.

where $R_{s,\mathrm{TEG}}$ is the internal electrical resistance of the TEG. Based on the current-voltage (I–V) characteristic of the TEG described in (6), the output power, $P_{\mathrm{TEG}}(V_{\mathrm{TEG}})$, delivered by the TEG to the load, R_L, can be determined. By substituting I_{TEG} with (6), the electrical power, $P_{\mathrm{TEG}}(V_{\mathrm{TEG}})$, harvested by the thermal energy harvester is derived as a function of its output voltage, V_{TEG}, which is expressed as

$$P_{\mathrm{TEG}}(V_{\mathrm{TEG}}) = V_{\mathrm{TEG}} * I_{\mathrm{TEG}} = \frac{V_{\mathrm{TEG}} * n * \alpha^{*}(T_H - T_C) - V_{\mathrm{TEG}}^2}{R_{s,\mathrm{TEG}}}. \quad (7)$$

Based on the technical specifications provided for the Thermo Life TEG [23], the TEG used in this paper is made up of 5200 thermocouples. Each thermocouple has a Seebeck's coefficient, α, of 0.21 mV/K and its internal electrical resistance, $R_{s,\mathrm{TEG}}$, is 82 kΩ. For a given temperature difference, $\Delta T = T_H - T_C$, between 5–10 K, the model illustrated by (7) is simulated for different TEG's output voltage, V_{TEG} and the simulation results are presented in Fig. 5. Experiments were carried out to characterize the TEG by applying a temperature difference between the thermal contact faces and both the electrical output voltage and current with different loads connected were measured. A hotplate is used to emulate the heat source and a Fluke 52-II digital thermometer with its thermocouple probe is used to measure the surface temperature. The output voltage and current are measured using two separate Fluke 8845A 6.5 digit precision multimeters and the measured parameters are used to calculate the electrical power. This experimental setup is used for harvesting energy under different thermal conditions with temperature differences in the range between 5 K and 10 K and the experimental results of the device under test, which is the TEG, are shown in Fig. 5.

Referring to the power curve (P–V) shown in Fig. 5, it can be seen that the simulation results obtained using the model expressed in (7) is comparable to the measurement results collected from the characterization of the thermal energy harvester under varying temperature differences. Fig. 5 shows that the maximum obtainable power for each thermal gradient corresponds to an output voltage of the thermal energy harvester i.e., $P_{\mathrm{MPPT},\Delta T=5K} = 96\ \mu\mathrm{W}$ @2.8 V, $P_{\mathrm{MPPT},\Delta T=10K} = 247\ \mu\mathrm{W}$ @4.5 V, etc. This is unlike the indoor solar energy harvesting case whereby all their power curves (P–V) peak near a particular output voltage of the solar panel (see Fig. 2).

However, this is not the case for another power curve (P–R) plotted for solar and thermal energy harvesting as shown in Figs. 3 and 6, respectively. It can be observed that the MPPs of the solar panel vary between the load resistances of 27–68 kΩ whereas the MPPs of the thermal energy harvester is fixed at the internal impedance of the thermal energy harvester of 82 kΩ. Fig. 6 shows that when the load resistance matches the source resistance of the thermal energy harvester, the harvested power is always maximum for different temperature differences. Because of that, it can be concluded from both power curves in Figs. 3 and 6 that no common MPPT approach exists between the solar and thermal energy harvesting systems.

III. Hybrid Energy Harvesting (HEH) From Solar and Thermal Energy Sources

The concept of HEH has been recently discussed in the literature [12]–[16] as a potential micro-power supply solution to minimize the size of the energy supply as well as to extend the operational lifetime of the wireless sensor node. Researchers have introduced a number of HEH methods to combine different small-scale energy harvesting (EH) sources. For these HEH methods, each EH source requires a unique power management circuit to condition the power flow from the energy source to its output load. The problem is that the number of converters used has to increase with multiple of the augmented energy sources. In this paper, this is not the case; the proposed HEH system requires only one power electronic based converter with a simple and low power control circuitry to condition the combined output power harvested simultaneously from the solar and thermal energy sources. By avoiding the use of different power management units for multiple energy sources, the number of components used in the HEH system are lessen and the system's form factor, cost and power losses are thus reduced. However, the challenge faced by this approach is that there could be impedance mismatch issue among the integrated energy sources.

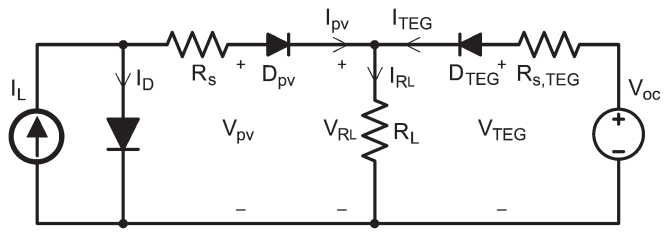

Fig. 7. Equivalent electrical circuit of the proposed hybrid energy harvester.

A. Characteristic of Solar Panel and Thermal Energy Harvester Connected in Parallel

For the HEH approach proposed in this paper, the terminal output voltages of the solar panel and the thermal energy harvester, $V_{\rm PV}$ and $V_{\rm TEG}$, respectively, are directly connected to the load, each via a schottky diode i.e., $D_{\rm PV}$ or $D_{\rm TEG}$ to block reverse-biased current flow. An overview of the equivalent electrical circuit of the hybrid energy harvester is shown in Fig. 7.

According to Figs. 2 and 5, the output voltages of the two energy sources are not that low, typically of few volts, hence the series energy sources configuration is not used to step-up the voltage across the load, V_{R_L}. Instead, a parallel energy sources configuration, $V_{R_L} = V_{\rm PV} + V_{D_{\rm PV}} = V_{\rm TEG} + V_{D_{\rm TEG}}$, is employed to produce more current flows i.e., $I_{R_L} = I_{\rm PV} + I_{\rm TEG}$. $V_{D_{\rm PV}}$ and $V_{D_{\rm TEG}}$ are the forward voltage drops of 0.2 V across each of the two series diodes. The power harvested from the solar panel, $P_{\rm PV}(V_{\rm PV})$, and the thermal energy harvester, $P_{\rm TEG}(V_{\rm TEG})$, expressed by (3) and (7), respectively, are summed together, and then subtracting with the power losses of the two series diodes, the resultant power is used to drive the load. The electrical power throughput of the hybrid energy harvester, $P_{\rm HEH}(V_{R_L})$, as a function of its output voltage, V_{R_L}, is thus given by

$$\begin{aligned} P_{\rm HEH}(V_{R_L}) &= |P_{\rm PV}(V_{R_L})| + |P_{\rm TEG}(V_{R_L})| \\ &\approx |V_{R_L} * I_{\rm sc,PV}| - \left| V_{R_L} * I_o \left[\exp\left(\frac{V_{R_L}}{n_s k T_c / q} \right) \right] \right| \\ &\quad + \left| \frac{V_{R_L} * V_{\rm oc,TEG} - V_{R_L}^2}{R_{s,\rm TEG}} \right|. \end{aligned} \tag{8}$$

Based on the technical specifications of the solar panel and the thermal energy harvester given in Sections II-B and II-C, respectively, the harvested power expression of the hybrid energy harvester, as expressed by (8), is simulated over a range of output voltages, V_{R_L}, for different solar irradiance and temperature differences that correspond to the solar panel's short-circuit current, $I_{\rm sc,PV}$, and the thermal energy harvester's open-circuit voltage, $V_{\rm oc,TEG}$. A set of the simulation and experimental results extracted under the minimum (380 lux and $\Delta T = 5$ K) and the maximum (1010 lux and $\Delta T = 10$ K) power harvesting conditions are shown in Fig. 8.

Referring to Fig. 8, it can be observed that the measured power curve (Measured $S + T$) of the hybrid energy harvester is the resultant of summing the individual power curves i.e., solar panel [Solar (S)] and thermal energy harvester [Thermal (T)]

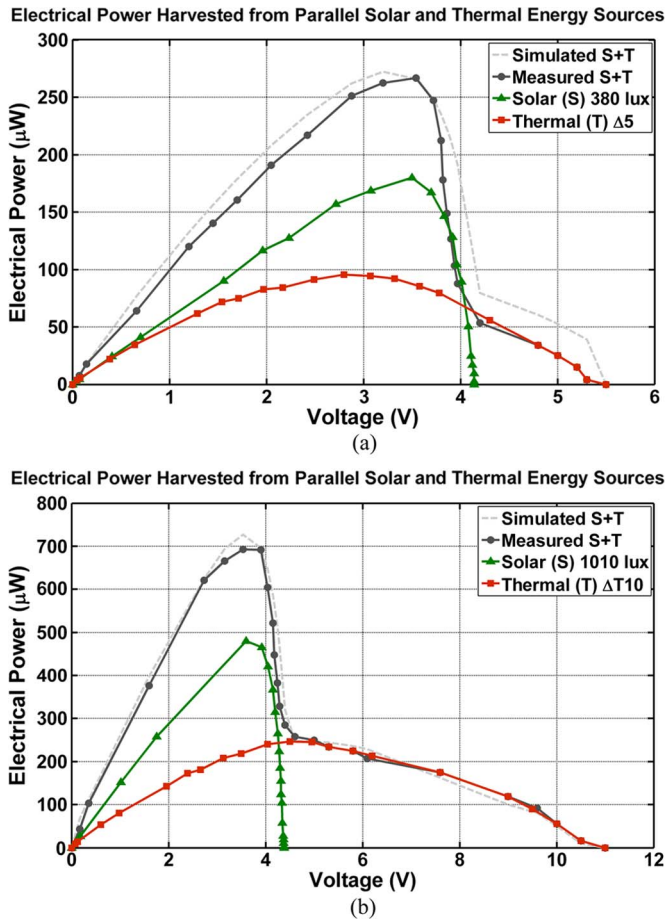

Fig. 8. Compare experimental harvested power with simulated power under the least and most power harvesting conditions (a) 380 lux and ΔT = 5 °C (top) and (b) 1010 lux and ΔT = 10 °C (bottom), respectively.

being superimposed into Fig. 8 minus the negligible small power loss in the schottky diodes. At MPPT voltage, $V_{R_L,\rm MPPT}$, of 3.6 V, the output voltages of the solar panel and thermal energy harvester are slightly higher than $V_{R_L,\rm MPPT}$ such that the two isolation diodes are conducting in the forward bias condition, hence, with reference to Fig. 8, it can be seen that the hybrid energy harvester can generate power at the minimum of 252 μW ($P_{\rm PV} = 167\ \mu$W, $P_{\rm TEG} = 85\ \mu$W) and at the maximum of 693 μW ($P_{\rm PV} = 466\ \mu$W, $P_{\rm TEG} = 227\ \mu$W), respectively. In addition, Fig. 8 shows that when $V_{RL} \geq V_{\rm PV}$, the solar panel operates in the open-circuit mode and therefore no solar power is harvested. This situation happens to the thermal energy harvester as well if $V_{R_L} \geq V_{\rm TEG}$ (3.6 V).

Another observation seen in Fig. 8 is that the simulated waveforms (Simulated S+T) based on the model expressed by (8) and the measured waveforms (Measured $S + T$) obtained from experiments are quite similar. The positive outcome of this observation verifies the expression model derived in (8), which can then be used to determine the electrical power throughput of the hybrid energy harvester, $P_{\rm HEH}$, to sustain the operational lifetime of the wireless sensor node. More analysis and characterization works were conducted on the hybrid energy harvester to evaluate the performance of the HEH system in powering the wireless sensor node. Figs. 9 and 10 show the power curves of the HEH system at fixed solar irradiance of

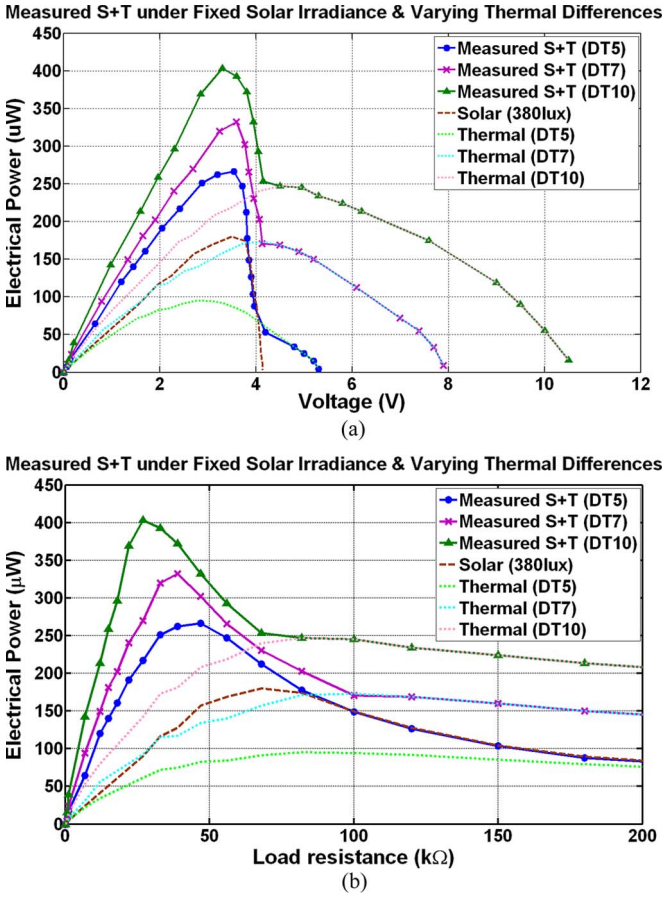

Fig. 9. P–V and P–R curves of HEH system at fixed solar irradiance of 380 lux(3 W/m^2) and different thermal conditions of 5–10 K.

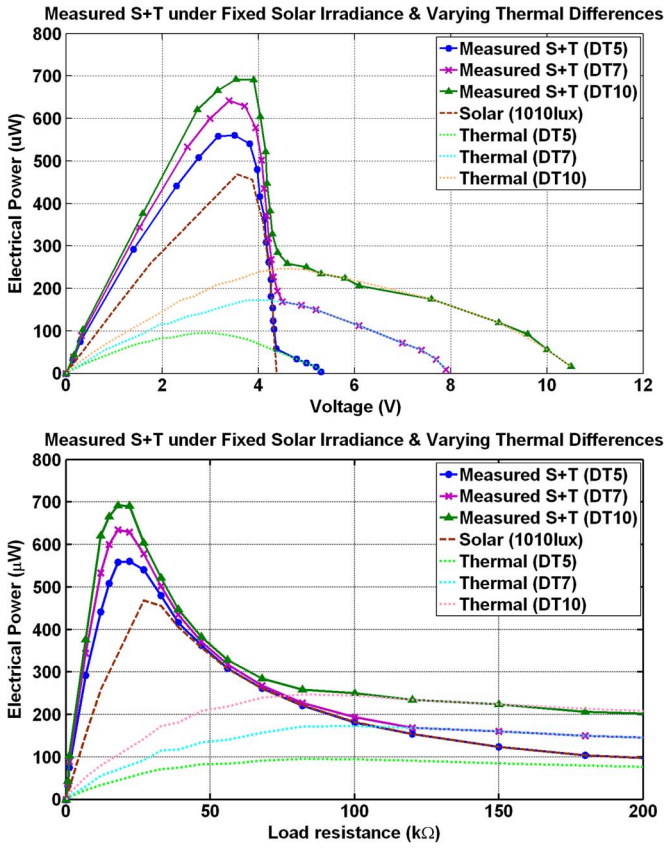

Fig. 10. P–V and P–R curves of HEH system at fixed solar irradiance of 1010 lux (3 W/m^2) and different thermal conditions of 5–10 K.

380 lux and 1010 lux, respectively, for varying thermal conditions in the range of 5–10 K. Conversely, the HEH system is also subjected to fixed thermal conditions of 5 K and 10 K, as shown in Figs. 11 and 12, respectively, for various solar irradiance between 380–1010 lux.

Referring to Figs. 9 and 10, it can be seen from the P–R curves (Thermal $\Delta T5$ − Thermal $\Delta T10$) that the MPPs of the stand-alone thermal energy harvester are fixed at its internal resistance of 82 kΩ under temperature differences in the range of 5–10 K. When the thermal energy harvester is paralleled with the solar panel under weak illumination of 380 lux and strong illumination of 1010 lux, it can be observed from the $P-R$ curves (Measured $S+T(\Delta T5)$ − Measured $S+T(\Delta T10)$) shown in Figs. 9 and 10 that the MPPs are not longer fixed, but vary with the combined internal impedance of the solar panel and the thermal energy harvester in parallel. This is the resulting effect of the impedance mismatch between the two energy sources of the hybrid energy harvester. Although there is impedance mismatch issue in the proposed HEH system, it is still possible to combine the two energy sources together without dedicating each individual energy source with a power converter to perform MPPT as proposed by Chulsung *et al.* in [16]. Referring to Figs. 9 and 10, the P–V curves (Measured $S+T(\Delta T5)$ − Measured $S+T(\Delta T10)$) show that all the MPPs of the hybrid energy harvester are fixed at around its output voltage of 3.6 V.

Likewise, for an illumination level of 380 lux and above as a common indoor lighting condition, the hybrid energy harvester tested under fixed thermal condition of 5 K and 10 K, as shown in Figs. 11 and 12, show that all of the P–V power curves (Measured $S+T(380\,\text{lux})$ − Measured $S+T(1010\,\text{lux})$ peak around 3.6 V. Reviewing through all the power curves shown in Figs. 9–12, it can be observed that all the MPPs of the P–V curves tend to cluster around a fixed voltage of 3.6 V, whereas the MPPs of the P–R curves are scattered out in the range of 20–50 kΩ. Hence, by deliberately setting the terminal voltage of the hybrid energy harvester to a value in the peak power range ($V_{R_L,\text{MPPT}} = 3.6$ V), it is possible to extract maximum output power from the hybrid energy harvester with a simple and ultra-low-power control circuit so as to place the panel at its MPPs, rather than using those energy hungry tracking techniques such as Perturb and Observe and Incremental Conductance, which require high computational power and cost.

B. Design and Implementation of Ultra-Low-Power Management Circuit

The schematic diagram of a self-autonomous indoor wireless sensor node powered by the proposed HEH system and its ultra-low-power power management circuit is illustrated in Fig. 13. Referring to Fig. 13, the designed power management circuitry with fixed voltage reference MPPT approach essentially consists of three main building blocks: 1) a boost converter with MPP tracker and its control and pulse width modulation (PWM)

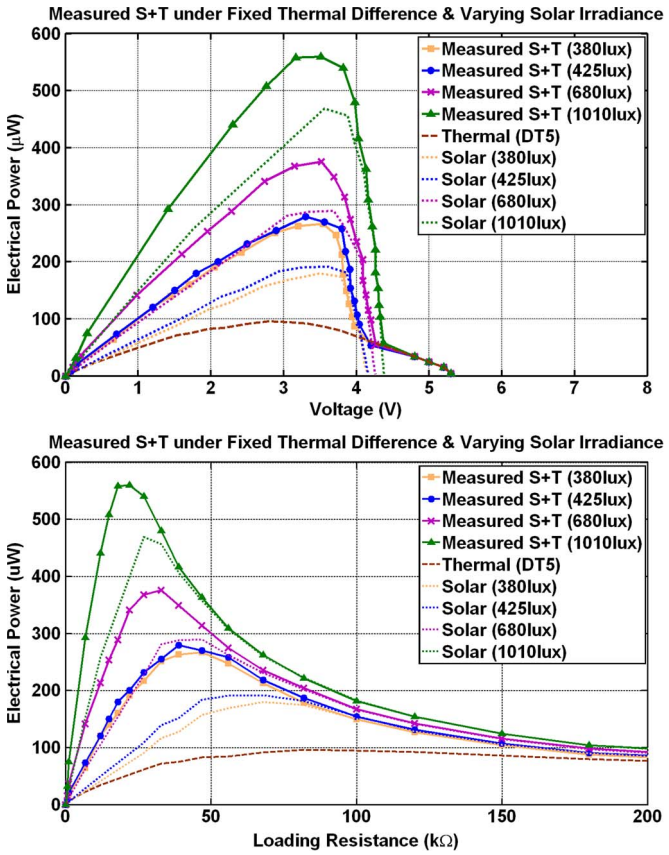

Fig. 11. P–V and P–R curves of HEH system at fixed thermal conditions of $\Delta T = 5$ K and varying solar irradiances of 380–1010 lux.

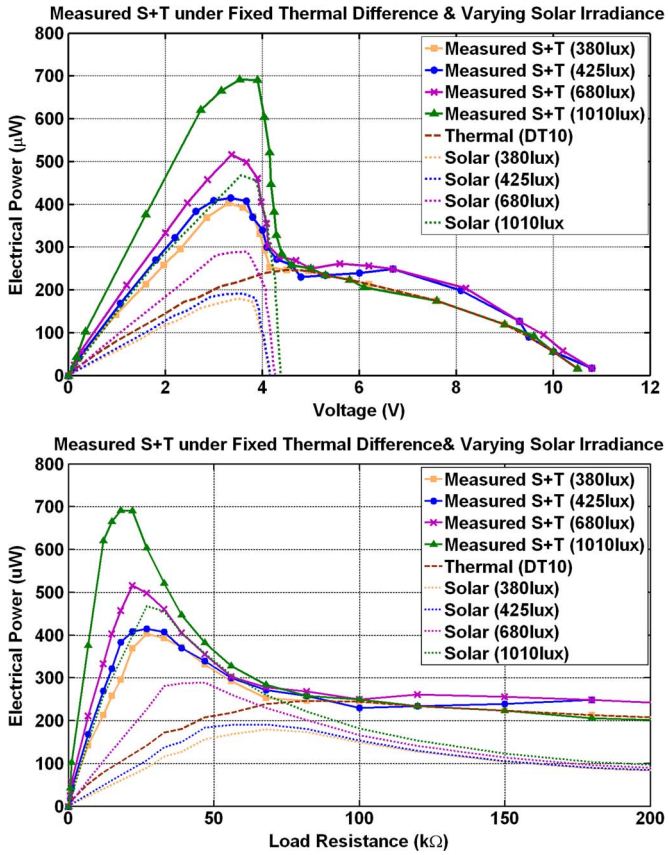

Fig. 12. P–V and P–R curves of HEH system at fixed thermal conditions of $\Delta T = 10$ K and varying solar irradiancesof 380–1010 lux.

generation circuit that manipulates the operating point of the HEH scheme to keep harvesting power at near MPPs; 2) an energy storage element i.e., supercapacitor to buffer the energy transfer between the source and the load; and 3) a regulating buck converter to provide constant voltage to the wireless sensor node and other electronic circuitries.

With reference to Fig. 13, the operation of the boost converter based on the fixed voltage reference approach is given as follows: the MPPT voltage reference signal, $V_{\rm MPPT}$, of 3.6 V is compared with the feedback voltage signal, V_{fb}, from the output of the hybrid energy harvester, which is also the input of the boost converter with voltage reference MPPT control. The resultant voltage error signal, $V_{\rm err}$, is fed into a proportional-integral (PI) controller that is embedded within a reduced clock speed Texas Instruments microcontroller (TI MSP430F2274) to generate a low frequency PWM signal, $\sim$100 Hz, for control of the boost converter. The algorithm implemented in the PI controller is designed based on the dynamic and steady state performance of the system, as shown in Fig. 14, where $V_{\rm in}$ and V_o are the input and output of the boost converter with MPPT control. Referring to Fig. 14, there is no overshoot as well as steady state error. The PI controller is characterized by a gain of $K_p = 0.3$ and a time constant of $T_I = 1/K_I = 10$ s.

By operating the TI microcontroller at lower clock speed, the power consumption of the microcontroller is significantly reduced to μW power level. However, in order to maintain the miniaturized size of the HEH system by using smaller passive components, the low frequency PWM control signal generated from the reduced clock speed microcontroller has to be transformed to a higher switching frequency of 10 kHz. This is achieved by designing an ultra-low-power PWM generation circuit made up of a micro-power resistor set oscillator (LTC6906) used for sawtooth generation and a micro-power, rail-to-rail CMOS comparator (LMC7215). The low frequency PWM signal, which represents the MPPT voltage reference, is filtered by a simple low-pass filter, 180 kΩ/4.7 μF, seen in Fig. 13. The dc signal obtained is then compared with the sawtooth wave to generate the duty cycle of the high frequency PWM control signal for the boost converter.

For indoor environment, the ambient energy sources such as solar and thermal gradient are not always available at all times and at a steady level, so there is a need to incorporate an energy storage device, i.e., supercapacitor, in the HEH system to store the excessive energy harvested from the solar panel and/or thermal energy harvester so as to buffer the indoor wireless sensor node for those times when energy sources are unavailable. Moreover, by drawing power simultaneously from both solar and thermal energy sources, the throughput power of the HEH system is increased which can enhance the performance of the indoor wireless sensor node. Supercapacitor is employed in this work because it has superior characteristics over batteries as described in [24]. These characteristics include numerous full charge cycles (more than half a million charge cycles), long lifetime (10–20 years operational lifetime) and high power density (an order of magnitude higher continuous current than a battery). Unlike the discrete capacitors which have very small

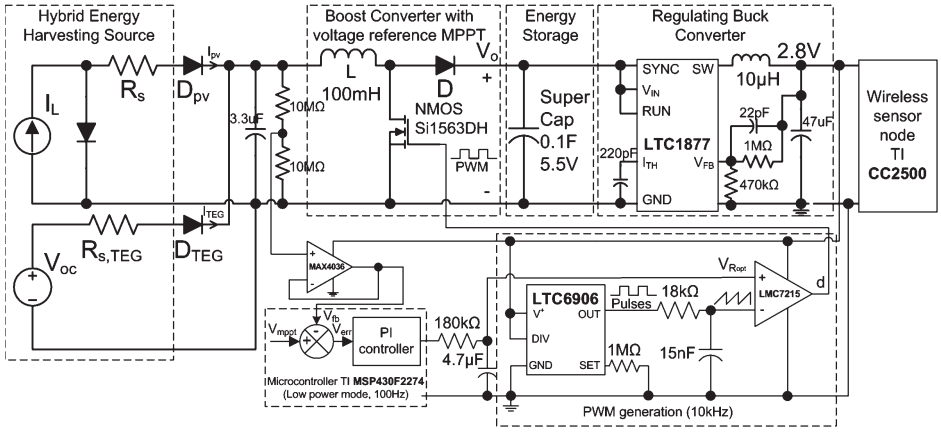

Fig. 13. Functional block diagram of HEH system.

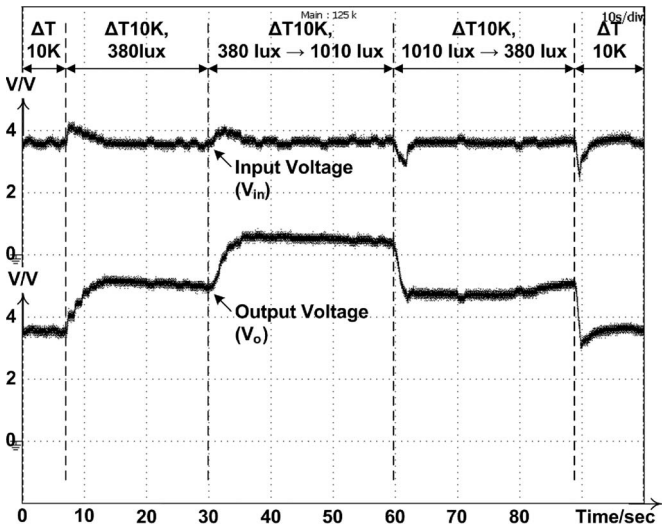

Fig. 14. Performance of ultra-low-power management circuit.

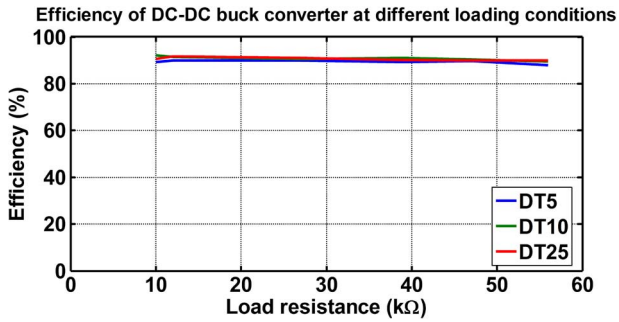

Fig. 15. Efficiency of regulating buck converter.

capacitance values of pF$-\mu$F range, the supercapacitor has very large capacitance value of Farads range suitable for energy storage purpose.

Lastly, the switched-mode voltage regulator (LTC1877) obtained from Linear Technology is inserted after the supercapacitor to provide a constant operating voltage of 2.8 V_{DC} to the wireless sensor node and other electronic circuitries. The efficiency of the regulating buck converter is experimentally tested, as shown in Fig. 15, to be around 80–90%, consuming an operating current of 12 μA. In this paper, the operation of the wireless sensor node deployed in an application field comprises: 1) sensing some external analog signals from sensory devices such as temperature, humidity, etc. and 2) communicating and relaying the sensed information to the gateway node in every 5 s time. Upon receiving the data at the base station, the collected data are then post-processed into usable information for any follow up action.

IV. Experimental Results

The near optimal HEH wireless sensor node has been successfully implemented into hardware prototype for laboratory testing. Several experimental tests have been conducted to analyze the performance of the HEH system and its simple and ultra-low-power fixed reference voltage MPPT scheme in powering the connected load consisting of the supercapacitor, the sensing, control and PWM generation circuitries and the wireless sensor node.

A. Performance of Parallel HEH Configuration

As mentioned before, when the solar and thermal energy sources of different characteristics are combined together, it is bound to have the issue of impedance mismatch among the integrated energy sources. As such, the performance of the parallel hybrid energy harvester, which contains the combined characteristics of the solar panel as well as the thermal energy harvester, is investigated. With reference back to Figs. 9–12, it is illustrated that the fixed reference voltage method is able to operate the hybrid energy harvester near its MPPs for different light intensities and temperature differences, but at the expense of some percentage of power loss in the harvested power. It is thus important to examine the significance of these power differences between the actual harvested power, $P_{\mathrm{HEH,actual}}$, with respect to the MPPs, $P_{\mathrm{HEH,MPPT}}$, of the hybrid energy harvester as recorded in Figs. 16 and 17.

Considering an extreme operating condition, which is at low light illumination of 380 lux and small temperature difference of 5 K as seen in Fig. 16, for example, the power harvested at the fixed reference MPPT voltage of 3.6 V, $P_{\mathrm{HEH,actual}}$, and the maximum obtainable power, $P_{\mathrm{HEH,MPPT}}$, of the hybrid energy harvester, are 252 μW and 260 μW, respectively. The power

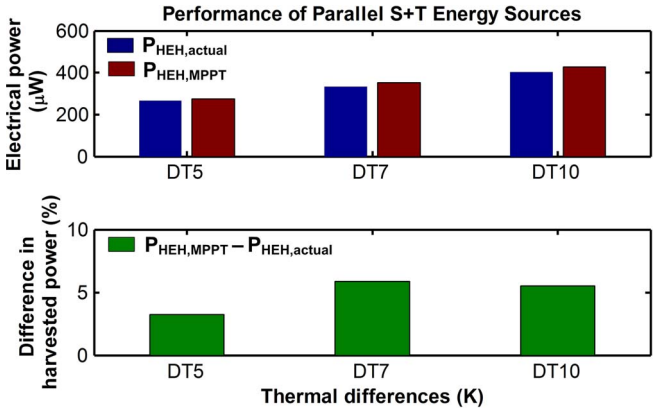

Fig. 16. Performance of HEH system in parallel configuration with varying thermal condition.

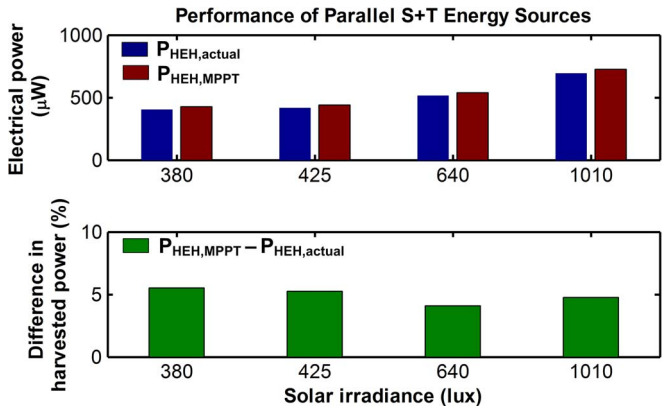

Fig. 17. Performance of HEH system in parallel configuration with varying solar irradiance.

difference is only 8 μW, which is about 3% of its harvested power as shown in Fig. 16. The power loss of 8 μW is due to the impedance mismatch issue between the solar panel and thermal energy harvester when they are connected directly without the use of separate power converters.

Similarly, referring to Figs. 16 and 17, it can be seen that the power differences between the actual harvested power, $P_{\mathrm{HEH,actual}}$, with respect to the MPPs, $P_{\mathrm{HEH,MPPT}}$, for all the other operating conditions range between 8–35 μW, which are 3–6% of the harvested power. Although the proposed HEH system i.e., hybrid energy harvester and its power management unit would incur power loss i.e., 8–35 μW in the overall harvested power, this power loss is so small and marginal as compared to those MPPT techniques that require high computational power and cost to fulfill their objective of precise and accurate MPP tracking. It is thus justifiable to utilize the simple and ultra-low-power fixed reference voltage method for the hybrid energy harvester.

B. Power Conversion Efficiency of HEH System

The power conversion efficiency of the HEH system is another important investigation being carried out. Other than the regulating buck converter, there are another two main contributors of power losses to the HEH system, namely the boost converter itself, which acts as a MPP tracker, and its associated

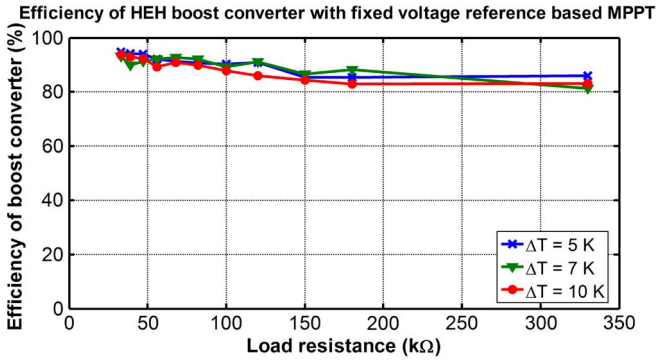

Fig. 18. Efficiency of HEH boost converter with varying temperature difference.

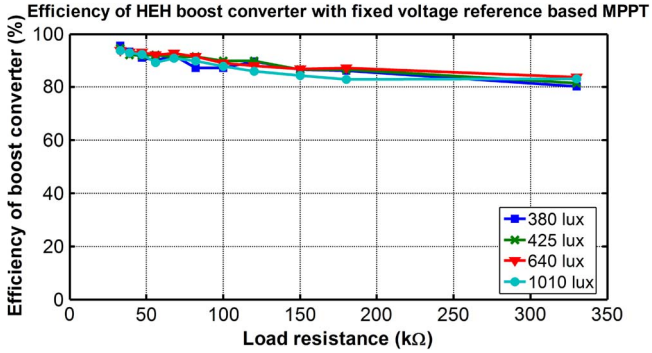

Fig. 19. Efficiency of HEH boost converter with varying solar irradiance.

sensing, control and PWM generation circuits. The efficiency of the boost converter, η_{conv}, can be expressed as a function of its output load power, P_{load}, over its input DC power, P_{dc}, under varying solar irradiance, temperature differences, ΔT, and loading, R_L, conditions. Take for example, at lux illumination, temperature difference and output load resistance of 380 lux, 5 K and 68 kΩ, respectively, the efficiency of the boost converter is given by

$$\eta_{\mathrm{conv}} = \frac{P_{\mathrm{out}}}{P_{\mathrm{in}}} * 100\% = \frac{V_{\mathrm{out}}^2/R_{\mathrm{load}}}{V_{\mathrm{in}} I_{\mathrm{in}}} * 100\% = \frac{4.95\ \mathrm{V}^2/68\ \mathrm{k\Omega}}{3.6\ \mathrm{V} * 109\ \mu\mathrm{A}} * 100\% = 91.8\% \quad (9)$$

and the calculated efficiency of 91.8% is plotted in Figs. 18 and 19. For all other temperature differences, solar irradiance and loading conditions, the efficiencies of the boost converter are calculated using (9) and the computed results are plotted in Figs. 18 and 19, respectively. It can observed from Figs. 18 and 19 that the efficiency of the designed boost converter ranges between 80% to 94% over a range of load resistances of 50–330 kΩ. At heavy load condition, say 50 kΩ, which signifies the discharge state of the supercapacitor, it can be seen in Figs. 18 and 19 that the efficiency of the boost converter is high, around 94%. This high-efficiency boost converter is very favorable and desirable to ensure optimal transfer of energy from the micropower sources of hundreds of microwatts or even lower to the energy storage.

As the loading gets lessen with the supercapacitor charges up, with reference to Figs. 18 and 19, it can be seen that the

efficiency of the converter decreases to around 82% at a load resistance of 300 kΩ. This decreasing efficiency trend is due to the power loss in the boost converter. Even so, the efficiency at light load is lower, it is not as critical as the heavy load condition because the supercapacitor, by then, is already near full charge state and any surplus energy would not be stored. Another source of power loss in the HEH system is the power consumption of the associated sensing, P_{sense}, control, P_{ctrl}, and PWM generation, P_{generate}, electronic circuits. Based on the voltage and current requirements of each individual component in the HEH system shown in Fig. 13, the total power consumption of the electronic circuits can be calculated as follows:

$$\begin{aligned} P_{\text{consumed}} &= P_{\text{sense}} + P_{\text{ctrl}} + P_{\text{PWM generate}} \\ &= 2.7\ \text{V} * (3\ \mu\text{A} + 15\ \mu\text{A} + 32\ \mu\text{A}) = 135\ \mu\text{W}. \end{aligned} \tag{10}$$

Once all the power losses in the HEH system are identified, including the power difference factor due to impedance mismatch between two paralleled energy sources and the power losses in the voltage regulating and MPPT converters, the performance of the designed HEH system for enhanced performance in the indoor wireless sensor node are evaluated.

In indoor applications like hospitals and factories, say the ambient condition is as follows: solar irradiance of 1010 lux and temperature difference of 10 K, referring back to Figs. 2 and 5 with operating conditions of 1010 lux and 10 K, the maximum power obtained by summing the individual MPP of the thermal energy harvester, P_{TEG}, and solar panel, P_{PV}, is 727 μW and the actual harvested power, $P_{\text{HEH,actual}}$, measured from the two paralleled energy sources is 690 μW. The power difference between the calculated and measured powers, due to impedance mismatch between two paralleled energy sources, is 35 μW as shown in Figs. 16 and 17. Taking into consideration both the power difference and the power losses in the voltage regulating and MPPT converters as shown in Figs. 18 and 19, the net harvested power output to power the indoor wireless sensor node through the boost converter with efficiency of 90% is 621 μW. This harvested power from the HEH system is more than what is harvested by the single-source energy harvesting system either from ambient light of 432 μW or thermal energy source of 223 μW, hence the significance of the proposed HEH system is exhibited. For a fully charged 0.1 F 5.5 V supercapacitor rechargeable by a single-source energy harvesting mechanism, either from ambient light or thermal energy source, the wireless sensor node, with an average power consumption of 1 mW, can last for around 0.74 or 0.54 hr, respectively. However, by using the proposed HEH system, the sensor lifetime is increased by around two times to 1.11 hours.

V. Conclusion

A near optimal HEH system has been proposed for enhanced performance of indoor wireless sensor node. Theoretical studies on individual as well as hybrid solar and thermal energy harvesting systems are conducted and simulated to understand the characteristic of the HEH system, which are then verified by experimental results. In this paper, the proposed HEH system using one power management circuit has successfully implemented into hardware prototype for laboratory testing. Based on the power analysis, the efficiency of the power management unit with fixed reference voltage based MPPT scheme is around 90% and its sensing, control and PWM generation circuitries consumes around 135 μW. Experimental results show that the HEH system can harvest an average electrical power of 621 μW from both energy sources at an average solar irradiance and thermal gradient of 1010 lux and 10 K, respectively, which is almost three times higher than the conventional single thermal energy harvesting method so as to enhance the performance of the indoor wireless sensor node.

References

[1] V. C. Gungor and G. P. Hancke, "Industrial wireless sensor networks: Challenges, design principles, and technical approaches," *IEEE Trans. Ind. Electron.*, vol. 56, no. 10, pp. 4258–4265, Oct. 2009.

[2] S. Roundy, E. S. Leland, J. Baker, E. Carleton, E. Reilly, E. Lai, B. Otis, J. M. Rabaey, P. K. Wright, and V. Sundararajan, "Improving power output for vibration-based energy scavengers," *IEEE Pervasive Comput.*, vol. 4, no. 1, pp. 28–36, Jan.–Mar. 2005.

[3] N. S. Hudak and G. G. Amatucci, "Small-scale energy harvesting through thermoelectric, vibration, and radio frequency power conversion," *J. Appl. Phys.*, vol. 103, no. 10, pp. 101301-1–101301-24, May 2008.

[4] Y. K. Tan and S. K. Panda, "Energy harvesting for autonomous wind sensor in remote area," in *Proc. 33rd IEEE IECON*, 2007, pp. 2104–2109.

[5] P. Glynne-Jones, M. J. Todor, S. P. Beeby, and N. M. White, "An electromagnetic, vibration-powered generator for intelligent sensor systems," *Sens. Actuators A, Phys.*, vol. 110, no. 1–3, pp. 344–349, Feb. 2004.

[6] D. Dondi, A. Bertacchini, D. Brunelli, L. Larcher, and L. Benini, "Modeling and optimization of a solar energy harvester system for self-powered wireless sensor networks," *IEEE Trans. Ind. Electron.*, vol. 55, no. 7, pp. 2759–2766, Jul. 2008.

[7] R.-Y. Kim, J.-S. Lai, B. York, and A. Koran, "Analysis and design of maximum power point tracking scheme for thermoelectric battery energy storage system," *IEEE Trans. Ind. Electron.*, vol. 56, no. 9, pp. 3709–3716, Sep. 2009.

[8] A. Nasiri, S. A. Zabalawi, and G. Mandic, "Indoor power harvesting using photovoltaic cells for low-power applications," *IEEE Trans. Ind. Electron.*, vol. 56, no. 11, pp. 4502–4509, Nov. 2009.

[9] A. Hande, T. Polk, W. Walker, and D. Bhatia, "Indoor solar energy harvesting for sensor network router nodes," *Microprocess. Microsyst.*, vol. 31, no. 6, pp. 420–432, Sep. 2007.

[10] J. F. Randall and J. Jacot, "Is AM1.5 applicable in practice? Modelling eight photovoltaic materials with respect to light intensity and two spectra," *Renew. Energy*, vol. 28, no. 12, pp. 1851–1864, Oct. 2003.

[11] J. F. Randall, *Designing Indoor Solar Products : Photovoltaic Technologies for AES*. Hoboken, NJ: Wiley, 2005.

[12] Y. Tadesse, S. Zhang, and S. Priya, "Multimodal energy harvesting system: Piezoelectric and electromagnetic," *J. Intell. Mater. Syst. Struct.*, vol. 20, no. 5, pp. 625–632, Mar. 2009.

[13] A. Khaligh, P. Zeng, and C. Zheng, "Kinetic energy harvesting using piezoelectric and electromagnetic technologies—State of the art," *IEEE Trans. Ind. Electron.*, vol. 57, no. 3, pp. 850–860, Mar. 2010.

[14] N. J. Guilar, T. J. Kleeburg, A. Chen, D. R. Yankelevich, and R. Amirtharajah, "Integrated solar energy harvesting and storage," *IEEE Trans. Very Large Scale Integr. (VLSI) Syst.*, vol. 17, no. 5, pp. 627–637, May 2009.

[15] H. Lhermet, C. Condemine, M. Plissonnier, R. Salot, P. Audebert, and M. Rosset, "Efficient power management circuit: From thermal energy harvesting to above-IC microbattery energy storage," *IEEE J. Solid-State Circuits*, vol. 43, no. 1, pp. 246–255, Jan. 2008.

[16] P. Chulsung and P. H. Chou, "AmbiMax: Autonomous energy harvesting platform for multi-supply wireless sensor nodes," in *Proc. 3rd IEEE Annu. Commun. Soc. SECON*, 2006, vol. 1, pp. 168–177.

[17] J. A. Paradiso and T. Starner, "Energy scavenging for mobile and wireless electronics," *IEEE Pervasive Comput.*, vol. 4, no. 1, pp. 18–27, Jan.–Mar. 2005.

[18] A. N. Celik and N. Acikgoz, "Modelling and experimental verification of the operating current of mono-crystalline photovoltaic modules using four- and five-parameter models," *Appl. Energy*, vol. 84, no. 1, pp. 1–15, Jan. 2007.

[19] M. G. Villalva, J. R. Gazoli, and E. R. Filho, "Comprehensive approach to modeling and simulation of photovoltaic arrays," *IEEE Trans. Power Electron.*, vol. 24, no. 5, pp. 1198–1208, May 2009.
[20] D. Sera, R. Teodorescu, and P. Rodriguez, "PV panel model based on datasheet values," in *Proc. IEEE Int. Symp. Ind. Electron.*, 2007, pp. 2392–2396.
[21] S. Dalola, M. Ferrari, V. Ferrari, M. Guizzetti, D. Marioli, and A. Taroni, "Characterization of thermoelectric modules for powering autonomous sensors," *IEEE Trans. Instrum. Meas.*, vol. 58, no. 1, pp. 99–107, Jan. 2009.
[22] A. Wickenheiser and E. Garcia, "Combined power harvesting from AC and DC sources," *Proc. SPIE*, vol. 7288, pp. 728816-1–728816-9, 2009.
[23] I. Stark, "Invited talk: Thermal energy harvesting with thermo life," in *Proc. Int. Workshop Wearable Implantable BSN*, 2006, pp. 19–22.
[24] F. I. Simjee and P. H. Chou, "Efficient charging of supercapacitors for extended lifetime of wireless sensor nodes," *IEEE Trans. Power Electron.*, vol. 23, no. 3, pp. 1526–1536, May 2008.

Yen Kheng Tan (S'02) received the B.Eng. degree in electrical and computer engineering from the National University of Singapore (NUS), Singapore, in 2003 and the Master of Technological Design (Mechatronics Engineering) degree jointly offered by NUS and the Eindhoven University of Technology (TU/e), Eindhoven, The Netherlands, in 2006. He is currently working toward the Ph.D. degree in electrical and computer engineering at NUS, Singapore.

His current research interest is on energy harvesting/scavenging for wireless sensor network (EH-WSN). In an EH-WSN, he works extensively on micro power generation using solar, wind, thermal and vibration energy sources, ultra-low-power analog-based and microcontroller-based optimal power (energy) management for wireless sensor nodes used for practical smart and sustainable applications.

Sanjib Kumar Panda (S'86–M'91–SM'01) received the B.Eng. degree in electrical engineering from REC, Surat, India, in 1983, the M.Tech. degree in electrical engineering from Institute of Technology, Benaras Hindu University, Varanasi, India, in 1987, and the Ph.D. degree in electrical engineering from the University of Cambridge, Cambridge, U.K., in 1991.

Since 1992, he has been a Faculty Member in the Department of Electrical and Computer Engineering, National University of Singapore, Singapore, where he is currently serving as Area Director of the Power & Energy Group. His research interests are in control of electric drives and power electronic converters, energy harvesting, renewable energy, assistive technology and mechatronics.

Dr. Panda received the Nehru Cambridge Fellowship jointly awarded by the Nehru Trust for Cambridge University, New Delhi, India, and Cambridge Commonwealth Trust, Cambridge, U.K., in 1987. He has served the IEEE Singapore Section for the past 18 years in various capacities at Chapter as well as at Section level, and as Section Chairman in 2003. He has served as the Conference Organizing Chairman for the IEEE Power Electronics and Drive Systems (PEDS'03) Conference and the Conference Organizing Chairman for the IEEE International Conference on Sustainable Energy Technologies (ICSET2008). He is also the recipient of the IEEE Third Millennium Medal.